

Graph-based methods coupled with specific distributional distances for adversarial attack detection

Dwight Nwaigwe^{1,2}, Lucrezia Carboni^{1,2}, Martial Mermillod³,
Sophie Achard¹, and Michel Dojat²

¹*Univ. Grenoble Alpes, Inria, CNRS, LJK. Grenoble. France*

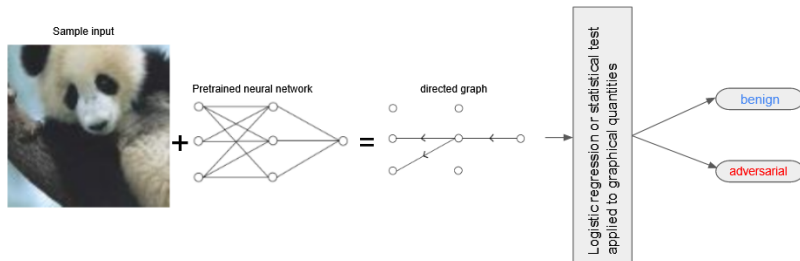
³*Univ. Grenoble Alpes, Univ. Savoie Mont Blanc, CNRS,
LPNC. Grenoble. France*

²*Univ. Grenoble Alpes, Inserm, U1216, Grenoble Institut
Neurosciences. Grenoble. France*

June 2, 2023

Abstract

Artificial neural networks are prone to being fooled by carefully perturbed inputs which cause an egregious misclassification. These *adversarial* attacks have been the focus of extensive research. Likewise, there has been an abundance of research in ways to detect and defend against them. We introduce a novel approach of detection and interpretation of adversarial attacks from a graph perspective. For an image, benign or adversarial, we study how a neural network’s architecture can induce an associated graph. We study this graph and introduce specific measures used to predict and interpret adversarial attacks. We show that graphs-based approaches help to investigate the inner workings of adversarial attacks.



1 Introduction

Artificial neural networks (ANN) are known to be prone to misclassifying carefully perturbed inputs [14]. These perturbed inputs, called adversarial, have been at the forefront of research in the machine learning community for the past decade. There is a lot of interest in creating new adversarial detection and defense methods, especially as this has consequence for a variety of real-world domains that rely on ANN for classification [8], [13], [31].

But among the known methods it is apparent that few of them, as diverse as they are, study adversarial attacks from a graph theory perspective. The objective of this paper is the exploration of adversarial attacks using graph-based methods. Indeed, the ANN structure can be described by a graph. In the most basic example, if one considers a standard feedforward ANN then, in a graphical representation, the neurons are associated to vertices/nodes and the weights between them are associated to edges. One may take this representation as inspiration for studying ANN from a graph perspective, although we stress that there is more than one way to obtain a graph from an ANN.

In [17], the authors provide a survey of the history of interactions between neuroscience and artificial intelligence and they note how much of the modern success in artificial intelligence can be traced to the understanding of or inspiration by biological systems. There is a line of research in neuroscience that studies the brain using elements of graph theory [4], and this provides some motivation for the use of graph-theoretic approaches to studying ANN.

In this document, we study the detection of adversarial examples using graphs. Given an input to the neural network, we compute an associated sparse graph. From this graph, we then use a combination of selected edges, an importance measure, and degree of nodes to predict if the input is adversarial. In one of our approaches, logistic regression is used. Our second

approach is statistical, being based on Wasserstein distance applied to degree of nodes. Lastly, we interpret the relative strength of attacks through our graph-based approach. An advantage of our detection methods is that they include a thresholding step which is non differentiable, thereby precluding gradient masking [28] and making it difficult to make adaptive attacks. As part of our studies we also provide benchmarks.

2 Background and related work

There have been some efforts in interpreting ANN in graph-theoretic ways. The authors of [32] study the existence and properties of *motifs*, clusters of neurons in ANN which appear often. In [18], they interpret ANN as a graph and study how MNIST and CIFAR datasets exhibit different distributions under defined quantities (e.g. node input strength, neuron strength). In [9], a topological study of ANN is made via its *functional graph*, a graph obtained from correlations of neurons. Other work [26],[23],[20] apply a similar topological view to studying ANN. Despite relating graphs to ANN, none of these articles demonstrate using graphs to detect adversarial examples, nor do they provide statistics on detection. An interesting use of graphs occurs in [6] where they are used to evaluate the robustness of an ANN, as opposed to adversarial detection. In [21] (“LID”), [19], [16], and [12], logistic regression is used to classify an input as benign or adversarial based on certain features, none of which are graph related. Statistical approaches can be found in [11] (“RSA”) and [29], also neither of which use graph methods. In [11], the distances between class prototypes are used to determine if an input is adversarial, while in [29], the authors claim that adding noise to images affects the logits in such a way that adversarial inputs can be detected. Our methods extend and complement the previous methods by showing the power of graph theory perspectives from either a logistic regression or a pure statistics perspective. We also compare our methods with LID and RSA.

3 Graph generation and quantities of interest

To compute the associated graph \mathcal{G} for a neural network and input pair, we use layerwise relevance propagation [2], [24]. This algorithm allows one to assign quantities to neurons which can be interpreted as an indicator of

the influence that a neuron has on the output. We assume our graph to be directed. Following the notation in [24] for the LRP- $\alpha\beta$ rule, signals are propagated from the output layer towards the input layers. For a neuron k in layer $\ell + 1$ that is connected to neuron i in layer ℓ , the propagated signal from k to i is defined to be

$$R_{i,k}^{\ell,\ell+1} = R_k^{\ell+1} \left(\alpha \frac{a_i \max(w_{ik}, 0)}{\epsilon + \sum_h a_h \max(w_{hk}, 0)} - \beta \frac{a_i \min(w_{ik}, 0)}{\epsilon + \sum_h a_h \min(w_{hk}, 0)} \right) \quad (1)$$

where R_k^ℓ is the relevance of neuron k , a_i is the activation of neuron i in layer ℓ ; w_{hk} is the weight between neurons h, k ; ϵ is a small parameter; and $\alpha - \beta = 1$. The relevance of a neuron k in layer l is given by

$$R_k^\ell = \sum_i R_{k,i}^{\ell,\ell+1}. \quad (2)$$

To start the algorithm, one assigns the relevance of the output neurons of the neural network to be equal to the neural network output. Upon completion of the algorithm, we rank the pairwise-relevance scores $\{R_{i,k}^{\ell,\ell+1}\}$ in descending order and keep the top 1%. Our thresholding is inspired by [4]. These edges become the edges in our induced graph \mathcal{G} . One can compute various quantities from \mathcal{G} . One such quantity is given by

$$I(v_i) = \sum_{j \neq i} \frac{1}{2^{d(v_i, v_j)}} \quad (3)$$

where $\{v_i\}_i$ is the set of nodes and $d(v_i, v_j)$ is the distance between vertices v_i, v_j . We note that for the distance between adjacent nodes we use (1), and the distance between any pair of nodes is given by the path that corresponds to the shortest sum of distances of adjacent nodes. An intuitive meaning of (3) is that it gives more importance to a vertex that has many neighbors and short distances to them. This equation is inspired by closeness centrality [3] which is given by

$$C(v_i) = \frac{1}{\sum_{j \neq i} d(v_i, v_j)}. \quad (4)$$

A difference between (3) and (4) is that the former is monotone in the cardinality of $\{v_i\}_i$. For bipartite graphs, or “stacks” of bipartite graphs (one can think of multi-layer perceptrons in this fashion) a measure of closeness centrality tends not be useful, hence the motivation for (3).

Another quantity of interest is the degree of a vertex, specifically which is defined to be the difference between out degree and in degree:

$$\text{deg}(v) = \text{deg}_{out}(v) - \text{deg}_{in}(v). \quad (5)$$

Our last quantity of interest are the values of certain edges of \mathcal{G} . This allows us to incorporate some of \mathcal{G} 's topology. The edges we use are those that correspond to the last two layers of the original neural network. We only use these edges because using all edges would require a data structure of size $O(n_1 n_2, \dots, n_l)$, where n_i is the number of nodes in layer i . Clearly, this requires an extensive amount of memory when a sufficient number of n_i is large. One can see that in general, when using graph data, it is preferable, at least from a memory standpoint, to use a quantity whose size is much smaller than $O(n_1 n_2, \dots, n_l)$, for instance a dataset whose size is $O(|V|)$, where V is the set of nodes. In fact, our use of degree and node importance (4) as computed for each node meets this constraint.

In [15], the neurons just before the softmax layer are studied, which has a similarity with our study of edge relevance. In that article, the authors use the said neurons to compare robustness of non-human primate and human vision with regards to adversarial images. This lends further a (biological) motivation in our use of edge relevance for the edges connecting the penultimate to the output layer. Since we apply a threshold to the edges of \mathcal{G} , there are nodes of \mathcal{G} which are not adjacent to an edge. More generally, the edges among the set $\{\mathcal{G}_i\}_i$, need not be the same, where $\{\mathcal{G}_i\}_i$ represents a set of graphs induced from the same architecture. To enforce consistency of representation for the relevance of edges adjacent to the output layer, we create a weighted adjacency matrix of the same dimension as the adjacency matrix for nodes in the last two layers. The relevance values that are above the threshold are recorded as is, and those below this percentile are set to 0. The matrix is then flattened into a vector. This flattened vector is our third quantity of interest, and its nonzero components are given by (1), assuming that component is greater than the threshold.

Lastly, we note that it would be very difficult to create an adaptive attack to counter the methodology proposed here since our detection methods involve graph thresholding, a nondifferentiable operation.

Table 1: Summary of relevant graph statistics. Edge relevance is restricted to last layer.

FORMULA	NAME
$R_{i,k}^{\ell,\ell+1} = R_k^{\ell+1} \left(\alpha \frac{a_i \max(w_{ik},0)}{\epsilon + \sum_h a_h \max(w_{hk},0)} - \beta \frac{a_i \min(w_{ik},0)}{\epsilon + \sum_h a_h \min(w_{hk},0)} \right)$	EDGE RELEVANCE
$I(v_i) = \sum_{j \neq i} \frac{1}{2^{d(v_i, v_j)}}$	NODE IMPORTANCE
$\text{deg} = \text{deg}_{out}(v) - \text{deg}_{in}(v)$	DEGREE

4 A statistical test based on Wasserstein distances

The Wasserstein-1 distance between two probability distributions p and q defined on a measurable metric space \mathcal{X} is given by

$$\mathcal{W}(p, q) = \min_{\pi(x,y) \in \Pi} \int \|x - y\|_1 d\pi(x, y) \quad (6)$$

where Π is the set of all measures on $(\mathcal{X}, \mathcal{X})$ whose marginal distributions are given by p and q . In the case when p consists of one sample x and q consists of discrete samples $(y_i)_{i=1}^N$, then

$$\mathcal{W}(\delta_x, q) = \frac{1}{N} \sum_i^N \|x - y_i\|_1. \quad (7)$$

where δ_x is the distribution with support at x . Wasserstein distances have been applied to machine learning in several ways. In [7], Wasserstein distances are used to compress data into a small dimensional subspace while maintaining a large distance from adversarial distributions. Other work [30] uses Wasserstein distances to create adversarial attacks.

Our goal in using Wasserstein distances is different than that in the examples mentioned. Our goal is to apply Wasserstein differences for benign and adversarial graph statistics in order to classify an input as benign or adversarial. The statistic we are concerned with is degree.

Let $\hat{\mathcal{B}}_i$ denote the empirical distribution of degree in the case when benign inputs are correctly classified as belonging to class i . Similarly, let $\hat{\mathcal{A}}_i$ denote

the empirical distribution that corresponds to perturbed inputs which the model incorrectly classifies as belonging to class i , and whose unperturbed image is correctly classified. For instance, since we are concerned with degree, the domain of the distribution function $\hat{\mathcal{B}}_i$ is a vector whose dimension is equal to the number of nodes in the induced graphs. If for some input, the model outputs class i , we would like to know if the output was generated by a random variable with distribution \mathcal{B}_i or with distribution \mathcal{A}_i where the lack of a hat denotes the true distribution. As before, we first construct the graph \mathcal{G} for the sample and compute a sample degree vector, which we denote by the random variable \mathbf{Z} . For a yet to be defined subset of nodes \mathcal{S} , we define the following Wasserstein Sums Ratio (WSR) quantity:

$$\text{WSR}(\mathcal{S}, \hat{\mathcal{A}}_i, \hat{\mathcal{B}}_i, \mathbf{Z}, i) = \frac{\sum_{j \in \mathcal{S}} \mathcal{W}(\delta_{\mathbf{z}_j}, \hat{\mathcal{B}}_i^j)}{\sum_{j \in \mathcal{S}} \mathcal{W}(\delta_{\mathbf{z}_j}, \hat{\mathcal{A}}_i^j)} \quad (8)$$

where the j in $\hat{\mathcal{A}}_i^j$ refers to the empirical distribution for node j , and similarly for $\hat{\mathcal{B}}_i^j$. Equation (8) says that for each node that belongs to \mathcal{S} , we compute Wasserstein-1 distances node-wise from the sample to the empirical distributions and we sum over the node indices, and compute the ratio. If the ratio is less than some threshold, we classify the input as benign, otherwise as adversarial. It may occur that the denominator of (8) is equal to 0, thus, in this case, a small term is added to the numerator and denominator. This can happen if the empirical distributions $\{\hat{\mathcal{A}}_i^j\}_{j \in \mathcal{S}}$ only have support at a point. Lastly, we note that we could have also computed the Wasserstein distance in \mathbb{R}^N , where N is the number of nodes in \mathcal{G} . However, that is a more involved procedure. Using (7), we can write (8) as

$$\text{WSR}(\mathcal{S}, \hat{\mathcal{A}}, \hat{\mathcal{B}}, \mathbf{Z}, i) = \frac{\frac{1}{N_{\hat{\mathcal{B}}_i^j}} \sum_{j \in \mathcal{S}} \sum_{k=1}^{N_{\hat{\mathcal{B}}_i^j}} \|\mathbf{Z}_j - y_i^j(k)\|_1}{\frac{1}{N_{\hat{\mathcal{A}}_i^j}} \sum_{j \in \mathcal{S}} \sum_{k=1}^{N_{\hat{\mathcal{A}}_i^j}} \|\mathbf{Z}_j - x_i^j(k)\|_1} \quad (9)$$

where $y_i^j(k)$ is a sample from $\hat{\mathcal{B}}_i^j$ and $x_i^j(k)$ is a sample from $\hat{\mathcal{A}}_i^j$, and $N_{\hat{\mathcal{B}}_i^j}$ is the number of samples in $\hat{\mathcal{B}}_i^j$, respectively for $\hat{\mathcal{A}}_i^j$. Lastly, we make the set \mathcal{S} as follows: we calculate

$$\Delta_i^j := \mathbb{E}X_i^j - \mathbb{E}Y_i^j \quad (10)$$

where X_i^j has distribution $\hat{\mathcal{A}}_i^j$ and Y_i^j has distribution $\hat{\mathcal{B}}_i^j$ and \mathbb{E} is expected

value. We then create the set

$$\mathcal{S} := \{j : \Delta_i^j < 0 \text{ for all } i\}. \quad (11)$$

The set \mathcal{S} identifies nodes where the mean of the benign distribution is greater than the adversarial distribution for all classes. Should it happen that $\hat{\mathcal{A}}_i^j$ is empty for some j (we have experienced this only for one combination of model and attack), one may create a placeholder version of it by setting each entry to a very large negative value (the large negative value has the effect of removing the index j from consideration when making the set \mathcal{S}). Algorithm 1 shows adversarial detection using WSR.

Algorithm 1 Adversarial detection using WSR (variant 1)

Input: neural network \mathcal{NN} , image I ; τ , \mathcal{S} , $\hat{\mathcal{A}}_i^j$; $\hat{\mathcal{B}}_i^j$ for all i and j
 $i \leftarrow \mathcal{NN}(I)$
 compute \mathcal{G} from I and \mathcal{NN}
 compute node degree \mathbf{z} from \mathcal{G}
 $val \leftarrow \text{WSR}(\mathcal{S}, \hat{\mathcal{A}}, \hat{\mathcal{B}}, \mathbf{z}, i)$
 if $val < \tau$ then classify I as benign, otherwise classify I as adversarial.

The way we construct \mathcal{S} has the tendency to pick nodes that generalize well across all classes at the expense of nodes that specialize. In an alternative algorithm, we propose to use the specialized nodes. For a given output that is classified as class i , we use $\mathcal{S}_i = \{j : \Delta_i^j < 0\}$. This can result in a more accurate test using our approach, but at the expense of a little longer computation since there are more nodes to use for computations. The algorithm is shown in Algorithm 2.

Algorithm 2 Adversarial detection using WSR (variant 2)

Input: neural network \mathcal{NN} , image I ; τ_i , \mathcal{S}_i , $\hat{\mathcal{A}}_i^j$; $\hat{\mathcal{B}}_i^j$ for all i and j
 $i \leftarrow \mathcal{NN}(I)$
 compute \mathcal{G} from I and \mathcal{NN}
 compute node degree \mathbf{z} from \mathcal{G}
 $val \leftarrow \text{WSR}(\mathcal{S}_i, \hat{\mathcal{A}}, \hat{\mathcal{B}}, \mathbf{z}, i)$
 if $val < \tau_i$ then classify I as benign, otherwise classify I as adversarial.

5 Consistency

We would like to analyze under what conditions (8) is a faithful predictor. We treat the case of a finite-width ANN with sufficiently many neurons. A finite-width ANN has the property that the degree distribution has compact support, which implies that the Wasserstein distance between an empirical degree distribution and true distribution is bounded, and the Wasserstein distance is continuous with respect to $\|\cdot\|_\infty$. We begin our proof of consistency by showing that given a real-valued random variable X ; an empirical distribution \hat{F}_n of some other real-valued random variable with true distribution F ; a function G (whose arguments are a random variable and a distribution) that is uniformly continuous in the second argument with respect to $\|\cdot\|_\infty$; and bounded, that

$$\mathbb{E}_X G(X, \hat{F}_n) \xrightarrow{a.s.} \mathbb{E}_X G(X, F) \quad (12)$$

as $n \rightarrow \infty$. To prove (12), it is sufficient to show that

$$G(X, \hat{F}_n) \xrightarrow{a.s.} G(X, F) \quad \forall x. \quad (13)$$

Under identical and independently distributed (iid) assumptions, the Glivenko-Cantelli lemma states that $\|\hat{F}_n - F\|_\infty \xrightarrow{a.s.} 0$. This combined with the uniform continuity of G in the second argument with respect to $\|\cdot\|_\infty$ proves (13). To prove (12), we let $h_n(x) = G(x, \hat{F}_n)$ and $h(x) = G(x, F)$. From (13) we have $h_n(x) \xrightarrow{a.s.} h(x)$ for all x as $n \rightarrow \infty$. We may combine this with the boundedness assumption to use the Lebesgue dominated convergence theorem, resulting in $\lim_{n \rightarrow \infty} \mathbb{E}_X h_n(X) = \mathbb{E}_X \lim_{n \rightarrow \infty} h_n(X) = \mathbb{E}_X h(X)$ almost surely.

We now begin to analyze (8), and we start by supposing that our random variable \mathbf{Z} corresponds to the benign case. Let

$$\begin{aligned} U_{j,i}^b &= \mathcal{W}(\delta_{\mathbf{z}_j}, \hat{\mathcal{B}}_i^j) \\ U_{j,i}^a &= \mathcal{W}(\delta_{\mathbf{z}_j}, \hat{\mathcal{A}}_i^j). \end{aligned} \quad (14)$$

For additional simplicity, let us assume that quantities defined in (14) are iid over the index j . The iid assumption implies that

$$\mathbf{E}_{\mathbf{z}_j} \mathcal{W}(\delta_{\mathbf{z}_j}, \hat{\mathcal{B}}_i^j) =: \mathbf{E}U_i^b$$

and

$$\mathbf{E}_{\mathbf{z}_j} \mathcal{W}(\delta_{\mathbf{z}_j}, \hat{\mathcal{A}}_i^j) =: \mathbf{E}U_i^a$$

for all i . By equation (12), the results we obtain going forward will hold for the population distribution in high probability assuming our empirical distributions have enough samples. By the weak law of large numbers,

$$\left| \frac{\sum_{j=1}^{|\mathcal{S}|} \mathcal{W}(\delta_{\mathbf{Z}_j}, \hat{\mathcal{B}}_i^j)}{|\mathcal{S}|} - \mathbf{E}U_i^b \right| < \epsilon_1 \text{ as } |\mathcal{S}| \rightarrow \infty$$

Similarly,

$$\left| \frac{\sum_{j=1}^{|\mathcal{S}|} \mathcal{W}(\delta_{\mathbf{Z}_j}, \hat{\mathcal{A}}_i^j)}{|\mathcal{S}|} - \mathbf{E}U_i^a \right| < \epsilon_2 \text{ as } |\mathcal{S}| \rightarrow \infty.$$

Then (8) is equal to

$$\begin{aligned} \frac{\sum_{j=1}^{|\mathcal{S}|} U_{j,i}^b}{\sum_{j=1}^{|\mathcal{S}|} U_{j,i}^a} &= \frac{|\mathcal{S}| \mathbf{E}U_i^b + |\mathcal{S}| \epsilon_1}{|\mathcal{S}| \mathbf{E}U_i^a + |\mathcal{S}| \epsilon_2} \\ &= \frac{\mathbf{E}U_i^b + \epsilon_1}{\mathbf{E}U_i^a + \epsilon_2} \\ &\rightarrow \frac{\mathbf{E}U_i^b}{\mathbf{E}U_i^a} \text{ as } |\mathcal{S}| \rightarrow \infty \end{aligned} \quad (15)$$

where ϵ_1 and ϵ_2 are $o(|\mathcal{S}|)$. If we consider the case when \mathbf{Z} is adversarial, we get a similar limit as in (15). Thus for consistency, we need the two limits to not be equal, thus we write

$$\frac{\mathbf{E}U_i^b}{\mathbf{E}U_i^a} < \frac{\mathbf{E}V_i^b}{\mathbf{E}V_i^a} \quad (16)$$

where we use V to denote adversarial quantities. This is equivalent to $\mathbf{E}U_i^b \mathbf{E}V_i^a < \mathbf{E}U_i^a \mathbf{E}V_i^b$. This is a realistic assumption for distributions with different means. A classification threshold, τ , is then picked such that

$$\frac{\mathbf{E}U_i^b}{\mathbf{E}U_i^a} < \tau < \frac{\mathbf{E}V_i^b}{\mathbf{E}V_i^a}. \quad (17)$$

An interesting example of (16) is the case in which $\mathbf{E}U_i^b = \mathbf{E}V_i^a$ and $\mathbf{E}U_i^a = \mathbf{E}V_i^b$ and where all terms do not equal 1. In this instance, (8) in the benign case will be the inverse of that in the adversarial case. Furthermore, neither ratio will equal 1. This happens when adversarial distributions are simply shifts of benign distributions.

Table 2: Architecture of Model 1

LAYER TYPE	OUTPUT SIZE	ACTIVATION FUNCTION
FULLY CONNECTED	300	ReLU
FULLY CONNECTED	200	ReLU
FULLY CONNECTED	150	ReLU
FULLY CONNECTED	150	ReLU
FULLY CONNECTED	100	SIGMOID
FULLY CONNECTED	10	SOFTMAX

6 Experimental details

6.1 Architectures

We experiment with five models, two of which are detailed in Tables 2-3 while the other three are VGG-19, InceptionResnetV2, and MobileNet. The last layers of VGG-19, InceptionResnetV2, and MobileNet are preloaded from Keras, and their last layers are replaced with three custom, fully-connected layers, with output sizes 4096, 1000, and 10, respectively, and trained with ImageNet weights. With respect to the last three models, we only compute graph-based quantities from these layers. For models 1 and 2, we use all layers.

6.2 Datasets

We trained our models on MNIST, CIFAR-10, and SVHN datasets. For each model we created adversarial examples using the Adversarial Robustness Toolbox [27]. For CIFAR-10 and SVHN, all images were enlarged to (224, 224, 3). Images were preprocessed using built-in Keras layers that handle input preprocessing.

Table 3: Architecture of Model 2

LAYER TYPE	OUTPUT SIZE	ACTIVATION FUNCTION
CONV	3 FILTERS, KERNEL SIZE (4,4)	IDENTITY
MAXPOOL	POOL SIZE=(2,2), STRIDES=(2,2)	ReLU
CONV	3 FILTERS, KERNEL SIZE (4,4)	IDENTITY
MAXPOOL	POOL SIZE=(2,2), STRIDES=(2,2)	ReLU
FULLY CONNECTED	100	ReLU
FULLY CONNECTED	10	SOFTMAX

6.3 Attacks

We consider fast gradient sign method, [14], projected gradient descent [22], untargeted Carlini-Wagner L2 [5], DeepFool [25], Square [1], and Auto [10] attacks. Fast gradient sign method attacks were clipped when perturbations were outside a ball of radius 10% in the ℓ^∞ norm. Projected gradient descent attacks were crafted using the same norm but with up to a 5% perturbation; the number of iterations was 40 except for InceptionResnetV2, MobileNet, and VGG19, in which 10 were used. Square and Auto attacks had the same norm and perturbation as projected gradient descent attacks. Optimization was done using ADAM with learning rate 0.01. For each attack we generated 10,000 adversarially perturbed images from 10,000 original (test data) images. In creating training data for the detection methods we introduce, approximately 14,000 samples were used, and the methods were compared on approximately 6,000 samples. For RSA the numbers are approximately the same. For LID, we used approximately 6,000 training and test samples each, with the exception of models 1 and 2 in which we used approximately 7,000 training and 3,000 test samples.

6.4 Hyperparameters

The values of ϵ and α in our implementation of LRP- $\alpha\beta$ are 2 and 10^{-7} , respectively. In our implementation of RSA we use $M = 8$, $K = 16$, and the layer used is the third from the output layer. For creating noisy samples in the algorithm in LID, we use Gaussian noise of zero mean and variance 0.05. Also in our implementation of LID, we only use the last 10 layers for

computational ease.

7 Results and discussion

7.1 Comparison of logistic regression approaches

In Tables 4a, 4b, and 4c we report the specificity (percentage benign samples that are correctly detected) and sensitivity (percentage adversarial samples that are correctly detected). One can see that the various graph statistics considered here can be strong sensitive and specific predictors of adversarial attacks in the case of using logistic regression. Among Mobilenet, Inception-ResnetV2 and VGG19, degree seems to slightly be the best predictor among our statistics. From the tables, we see that the worst performance occurs for Carlini-Wagner and Deepfool attacks. These two attacks are known to be among the most difficult to detect, so our results are consistent with this belief. In particular, for VGG19 and Carlini-Wagner, our classifier is able to almost always detect benign samples, but detects almost no adversarial examples.

Among models 1 and 2, degree is significantly the best predictor, while edge relevance for Model 2 is a poor predictor across all attacks, being unable to detect adversarial images. This is because the edge relevance for benign and adversarial samples are equal to 0. The largest relevances for Model 2 are found in layers closer to the input layer. During the thresholding process, the relevances for the edges corresponding to the output layer are set to 0 because they are relatively small. Lastly, in comparison to LID, our results are superior across almost all model/attack combinations.

7.2 Comparison of statistical approaches

Tables 5a, 5b, and 5c show results in terms of AUROC (area under receiver operating characteristic curve) for various detection methods. In almost all cases, WSR2 provides more accurate predictions than WSR1. Further, both WSR variations outperform RSA. Model 1, in comparison to the other models, performs somewhat poorly under WSR1. This seems to be due to Model 1 having the least number of neurons, making the corresponding $|\mathcal{S}|$ relatively small. On this note, we can also see from the tables that model/attack pairs with small $|\mathcal{S}|$ tend to have worse results under WSR.

model		Attack					
		FGSM	PGD	CW2	DF	Sq	AA
MobileNet	degree	99.64/98.10	99.63/99.23	82.21/90.74	80.23/91.34	94.08/93.22	100/99.63
	node importance	99.52/99.35	99.46/100	64.50/99.43	66.78/93.91	91.86/93.39	99.89/100
	edge relevance	100/99.98	99.71/99.61	85.27/90.06	87.75/89.24	100/99.85	100/99.86
	LID	23.49/85.93	12.01/97.90	22.30/79.84	35.59/68.10	24.47/98.60	7.02/87.35
InceptionResNetV2	degree	100/99.95	100/99.92	84.05/94.31	73.88/86.22	96.18/98.50	99.66/100
	node importance	100/100	100/100	65.76/88.13	44.12/96.08	89.30/99.36	100/99.96
	edge relevance	99.96/99.70	100/99.70	80.36/78.76	80.96/74.43	99.21/96.59	100/99.78
	LID	40.13/66.23	76.58/44.09	21.08/73.91	72.97/28.78	67.79/41.59	31.60/75.93
VGG19	degree	100/99.86	99.92/99.73	99.77/04.20	97.55/99.08	98.98/98.21	99.16/100
	node importance	99.96/100	99.96/100	100/0.7	94.88/99.35	98.24/98.28	97.97/100
	edge relevance	99.73/99.72	99.96/99.96	100/0	99.66/96.82	99.66/97.21	100/99.92
	LID	79.66/6.57	99.39/42.71	41.77/57.55	99.73/0.88	98.78/0.11	22.14/76.08

(a) Cifar-10

model		Attack					
		FGSM	PGD	CW2	DF	Sq	AA
MobileNet	degree	100/100	100/99.77	77.25/91.87	55.44/92.96	99.66/99.04	100/100
	node importance	100/100	99.66/100	55.61/90.53	54.39/88.69	89.30/99.36	100/99.96
	edge relevance	100/99.79	100/99.85	99.59/76.24	79.85/74.90	99.21/96.96	100/99.81
	LID	57.12/40.29	69.78/37.14	77.47/23.03	92.97/7.03	88.45/7.71	85.23/37.52
InceptionResNetV2	degree	99.88/99.84	98.63/100	76.00/91.52	75.29/92.63	87.35/97.11	99.41/100
	node importance	100/100	100/99.96	45.68/93.81	89.52/94.36	89.52/94.36	100/100
	edge relevance	99.96/99.68	100/99.60	74.06/76.25	92.95/90.58	92.95/90.58	100/99.92
	LID	92.14/4.10	69.78/37.14	77.17/23.02	53.32/48.55	29.87/59.27	10.75/61.80
VGG19	degree	100/99.93	100/100	97.67/29.68	98.80/99.18	96.97/99.57	99.96/100
	node importance	100/99.94	100/99.96	98.84/9.68	99.34/99.39	98.64/99.73	100/100
	edge relevance	100/99.88	100/99.81	100/0	99.96/98.37	100/97.83	100/99.92
	LID	67.79/40.38	2.26/85.83	42.24/47.81	4.14/92.37	7.01/98.72	6.47/29.00

(b) SVHN

model		Attack					
		FGSM	PGD	CW2	DF	Sq	AA
Model 2	degree	99.00/95.45	99.90/95.45	98.05/99.19	97.26/99.20	99.86/65.44	99.97/95.34
	node importance	84.80/24.54	92.79/12.46	52.75/62.37	34.22/73.53	97.71/5.53	94.50/8.04
	edge relevance	100/0	100/0	100/0	100/0	100/0	100/0
	LID	81.94/13.43	88.19/10.41	74.90/21.72	71.79/22.27	52.77/50.96	16.10/87.53
Model 1	degree	95.96/98.91	94.76/84.19	6.58/88.76	95.51/96.71	98.63/71.97	96.02/84.48
	node importance	81.67/96.19	96.09/54.83	0.14/99.70	88.14/96.57	100/2.09	93.87/60.39
	edge relevance	90.34/86.50	89.31/85.25	49.55/42.19	95.68/93.58	100/0	89.47/88.57
	LID	50.60/49.75	72.07/25.38	47.20/55.53	71.79/22.27	52.77/50.96	26.71/72.12

(c) MNIST

Table 4: Comparison between logistic regression methods. First and second quantities in each entry are benign and adversarial detection rate, respectively. FGSM, PGD, CW2, DF, Sq, and AA represent fast gradient sign method, projected gradient descent, Carlini-Wagner L2, Square, and Auto attacks, respectively. Values are percentages.

This is particularly noticeable in the case of Carlini-Wagner and Deepfool attacks under WSR1; this lower performance was also noted in our results using logistic regression.

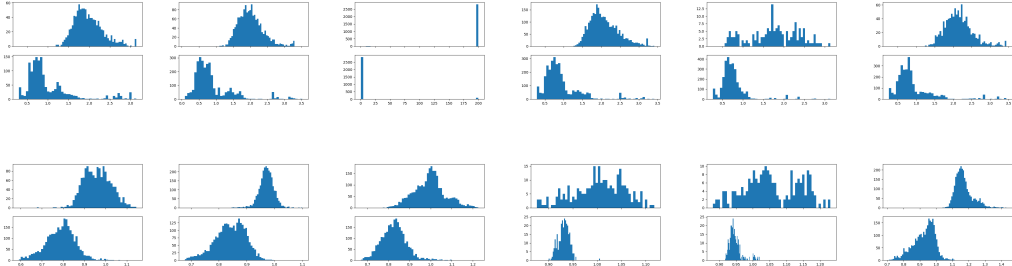


Figure 1: Empirical distributions for WSR1 for Model 2 (top row) and WSR2 for InceptionResnetV2 (bottom row). The top panel of each subplot shows WSR computed for adversarial examples, and the bottom subplot shows the computation for benign examples. FGSM, PGD, CW2, DF, Sq, and AA represent fast gradient sign method, projected gradient descent, Carlini-Wagner L2, Deepfool, Square, and Auto attacks, respectively. For Model 2 and CW2, values above 200 are set to 200 for ease of display. Note that the benign and adversarial plots for Model 2 tend to agree with the remark made in section 1 about inverses.

We can use WSR and logistic regression in a complementary way. For instance, graph-based quantities generated from VGG19 and Carlini-Wagner attacks tend to be poorly classified with logistic regression. In contrast, WSR2 performs well in this case, and it can be used in place of logistic regression.

We considered using equation 5 from [29] as a baseline, perhaps in place of RSA, but chose not to because of the extremely large time needed for the source code to run, and secondly, our initial results suggested that this method gives poor accuracy, near 50%, which is much lower than the numbers the article states. In our effort to increase accuracy we experimented with different hyperparameters, including noise, but to no avail. This calls into question the usefulness and robustness of using equation 5 in [29].

7.3 Nodal analysis

The distributions of node quantities is highly dependent on the model and attack. From the tables it can be seen that AUROC for WSR decreases as the strength of the attack increases (we consider a partial order of increasing attack strength to be: Fast Gradient Sign Method, Projected Gradient Descent, and Carlini-Wagner L2). We can relate this observation to how the cardinality of $|\mathcal{S}|$ varies with model/attack. The cardinality of $|\mathcal{S}|$ can be seen in Tables 6a,6b, and 6c. For CIFAR-10 and SVHN datasets, we observe that the cardinality tends to be a lot smaller for Carlini-Wagner L2 and DeepFool attacks, and it seems to explain the lower accuracy achieved by WSR on these attacks. We recall that from section 5, the accuracy of WSR increases with $|\mathcal{S}|$.

We also note that in some cases the benign distribution of WSR and the adversarial distribution of WSR are centered at points which are close to inverses. This seems to be the case for Model 2, as shown in figure 1. This is in agreement with an earlier remark in Section 5 about equation (8) having inverse values under benign and adversarial examples, assuming the benign and adversarial test statistics have the same distributions up to a shift.

		Attack						
		FGSM	PGD	CW2	DF	Sq	AA	
model	MobileNet	WSR1	99.98	100	79.78	73.56	92.98	100
		WSR2	100	94.47	98.00	92.11	99.25	100
		RSA	51.31	68.56	84.94	48.79	97.44	85.74
model	InceptionResNetV2	WSR1	99.64	99.00	81.46	64.23	84.88	100
		WSR2	97.26	99.05	95.69	88.54	89.93	99.98
		RSA	94.67	98.89	99.06	98.59	98.72	95.07
model	VGG19	WSR1	100	99.98	74.83	98.78	97.08	99.98
		WSR2	99.87	99.97	97.36	99.32	99.70	100
		RSA	69.08	54.28	71.70	73.77	76.58	63.78

(a) Cifar-10

		Attack						
		FGSM	PGD	CW2	DF	Sq	AA	
model	MobileNet	WSR1	100	100	81.62	78.95	99.29	100
		WSR2	100	100	95.20	90.26	99.80	100
		RSA	80.12	63.12	87.69	82.83	76.48	82.27
model	InceptionResNetV2	WSR1	100	100	78.35	80.59	92.12	100
		WSR2	99.86	99.91	93.84	94.29	96.81	100
		RSA	51.77	61.81	56.35	60.25	58.44	58.19
model	VGG19	WSR1	100	100	76.33	99.65	99.54	100
		WSR2	100	100	94.57	99.68	99.87	100
		RSA	80.69	57.27	76.79	79.63	81.77	58.23

(b) SVHN

		Attack						
		FGSM	PGD	CW2	DF	Sq	AA	
model	Model 2	WSR1	95.16	95.37	96.48	95.44	91.77	95.54
		WSR2	96.75	96.23	96.73	96.08	91.74	96.68
		RSA	66.81	62.81	58.54	55.95	68.33	63.12
model	Model 1	WSR1	95.53	81.06	41.25	82.48	89.3	83.6
		WSR2	96.36	94.40	39.65	97.81	99.48	94.36
		RSA	71.80	72.10	51.64	89.60	96.34	71.85

(c) MNIST

Table 5: Comparison of AUROC for statistical detection methods. FGSM, PGD, CW2, DF, Sq, and AA represent fast gradient sign method, projected gradient descent, Carlini-Wagner L2, Deepfool, Square, and Auto attacks, respectively. WSR1 and WSR2 are WSR variants 1 and 2 respectively. Values are percentages.

model		Attack					
		FGSM	PGD	CW2	DF	Sq	AA
MobileNet	WSR1	877	734	51	68	405	79
InceptionResnetV2	WSR1	378	484	109	180	240	120
VGG19	WSR1	180	776	34	925	692	578

(a) Cifar-10

model		Attack					
		FGSM	PGD	CW2	DF	Sq	AA
MobileNet	WSR1	422	636	78	97	551	287
InceptionResnetV2	WSR1	754	1269	109	160	922	496
VGG19	WSR1	945	1253	63	1379	929	843

(b) SVHN

model		Attack					
		FGSM	PGD	CW2	DF	Sq	AA
Model 2	WSR1	129	105	50	34	52	115
Model 1	WSR1	33	10	7	5	4	10

(c) MNIST

Table 6: Cardinality of \mathcal{S} by model and attack. FFGSM, PGD, CW2, DF, Sq, and AA represent fast gradient sign method, projected gradient descent, Carlini-Wagner L2, Deepfool, Square, and Auto attacks, respectively.

8 Conclusion

We have demonstrated that neural network architectures can be interpreted in a graph context from which we can use the statistics of graph-based quantities to detect adversarial attacks. We introduced three measures that we applied to our graphs and used them as predictors of adversarial attack. We showed that this approach can produce high detection performances with logistic regression. We also studied the distributions of node degree using a statistical test based on Wasserstein distances. We find it intriguing that a sparse graph encodes sufficient information about inputs to a neural network. We hope that the perspective introduced here will provide a different way of understanding adversarial attacks.

9 Acknowledgments

L. Carboni and D. Nwaigwe are the recipients of a grant from MIAI@Grenoble Alpes (ANR 19-P3IA-003).

References

- [1] Maksym Andriushchenko, Francesco Croce, Nicolas Flammarion, and Matthias Hein. Square attack: A query-efficient black-box adversarial attack via random search. In *Computer Vision - ECCV 2020 - 16th European Conference, Glasgow, UK, August 23-28, 2020, Proceedings, Part XXIII*, volume 12368 of *Lecture Notes in Computer Science*, pages 484–501. Springer, 2020.
- [2] Sebastian Bach, Alexander Binder, Grégoire Montavon, Frederick Klauschen, Klaus-Robert Müller, and Wojciech Samek. On Pixel-Wise Explanations for Non-Linear Classifier Decisions by Layer-Wise Relevance Propagation. *PLOS ONE*, 10(7):e0130140, July 2015.
- [3] Alex Bavelas. Communication patterns in task-oriented groups. *The Journal of the Acoustical Society of America*, 22(6):725–730, 1950.
- [4] Ed Bullmore and Olaf Sporns. Complex brain networks: graph theoretical analysis of structural and functional systems. *Nature Reviews Neuroscience*, 10(3):186–198, March 2009.
- [5] Nicholas Carlini and David Wagner. Towards evaluating the robustness of neural networks. In *2017 IEEE Symposium on Security and Privacy (SP)*, pages 39–57, 2017.
- [6] Wuxinlin Cheng, Chenhui Deng, Zhiqiang Zhao, Yaohui Cai, Zhiru Zhang, and Zhuo Feng. Spade: A spectral method for black-box adversarial robustness evaluation. In *Proceedings of the 38th International Conference on Machine Learning*, volume 139 of *Proceedings of Machine Learning Research*, pages 1814–1824. PMLR, 18–24 July 2021.
- [7] Anoop Cherian and Shuchin Aeron. Representation learning via adversarially-contrastive optimal transport. In *Proceedings of the 37th International Conference on Machine Learning*, Proceedings of Machine Learning Research. PMLR, 2020.
- [8] Dan Cireşan, Ueli Meier, Jonathan Masci, and Jürgen Schmidhuber. Multi-column deep neural network for traffic sign classification. *Neural Networks*, 32:333–338, 2012. Selected Papers from IJCNN 2011.

- [9] Ciprian A. Corneanu, Meysam Madadi, Sergio Escalera, and Aleix M. Martinez. What does it mean to learn in deep networks? And, how does one detect adversarial attacks? In *2019 IEEE/CVF Conference on Computer Vision and Pattern Recognition (CVPR)*, pages 4752–4761, 2019.
- [10] Francesco Croce and Matthias Hein. Reliable evaluation of adversarial robustness with an ensemble of diverse parameter-free attacks. In *Proceedings of the 37th International Conference on Machine Learning, ICML 2020, 13-18 July 2020, Virtual Event*, volume 119 of *Proceedings of Machine Learning Research*, pages 2206–2216. PMLR, 2020.
- [11] Nathan Drenkow, Neil Fendley, and Philippe Burlina. Attack agnostic detection of adversarial examples via random subspace analysis. In *IEEE/CVF Winter Conference on Applications of Computer Vision, WACV 2022, Waikoloa, HI, USA, January 3-8, 2022*, pages 2815–2825. IEEE, 2022.
- [12] Reuben Feinman, Ryan R. Curtin, Saurabh Shintre, and Andrew B. Gardner. Detecting adversarial samples from artifacts. *arXiv preprint ARXIV.1703.00410*, 2017.
- [13] Samuel G. Finlayson, John D. Bowers, Joichi Ito, Jonathan L. Zittrain, Andrew L. Beam, and Isaac S. Kohane. Adversarial attacks on medical machine learning. *Science*, 363(6433):1287–1289, 2019.
- [14] Ian J. Goodfellow, Jonathon Shlens, and Christian Szegedy. Explaining and harnessing adversarial examples. In *3rd International Conference on Learning Representations*, 2015.
- [15] Chong Guo, Michael Lee, Guillaume Leclerc, Joel Dapello, Yug Rao, Aleksander Madry, and James Dicarlo. Adversarially trained neural representations are already as robust as biological neural representations. In *Proceedings of the 39th International Conference on Machine Learning*, volume 162 of *Proceedings of Machine Learning Research*, pages 8072–8081. PMLR, 17–23 Jul 2022.
- [16] Paula Harder, Franz-Josef Pfrendt, Margret Keuper, and Janis Keuper. SpectralDefense: Detecting Adversarial Attacks on CNNs in the Fourier

- Domain. In *2021 International Joint Conference on Neural Networks (IJCNN)*, pages 1–8, Shenzhen, China, Jul 2021. IEEE.
- [17] Demis Hassabis, Dhharshan Kumaran, Christopher Summerfield, and Matthew Botvinick. Neuroscience-Inspired Artificial Intelligence. *Neuron*, 95(2):245–258, July 2017.
- [18] Emanuele La Malfa, Gabriele La Malfa, Claudio Caprioli, Giuseppe Nicosia, and Vito Latora. Deep neural networks as complex networks. *arXiv preprint ARXIV.2209.05488*, 2022.
- [19] Kimin Lee, Kibok Lee, Honglak Lee, and Jinwoo Shin. A simple unified framework for detecting out-of-distribution samples and adversarial attacks. In *Advances in Neural Information Processing Systems 31: Annual Conference on Neural Information Processing Systems*, pages 7167–7177, 2018.
- [20] Shiwei Liu, Tim van der Lee, Anil Yaman, Zahra Atashgahi, Davide Ferraro, Ghada Sokar, Mykola Pechenizkiy, and Decebal Constantin Mocanu. Topological insights into sparse neural networks. In *Machine Learning and Knowledge Discovery in Databases - European Conference, ECML PKDD 2020, Ghent, Belgium, September 14-18, 2020, Proceedings, Part III*, volume 12459 of *Lecture Notes in Computer Science*, pages 279–294. Springer, 2020.
- [21] Xingjun Ma, Bo Li, Yisen Wang, Sarah M. Erfani, Sudanthi N. R. Wijewickrema, Grant Schoenebeck, Dawn Song, Michael E. Houle, and James Bailey. Characterizing adversarial subspaces using local intrinsic dimensionality. In *6th International Conference on Learning Representations, ICLR 2018, Vancouver, BC, Canada, April 30 - May 3, 2018, Conference Track Proceedings*. OpenReview.net, 2018.
- [22] Aleksander Madry, Aleksandar Makelov, Ludwig Schmidt, Dimitris Tsipras, and Adrian Vladu. Towards deep learning models resistant to adversarial attacks. In *International Conference on Learning Representations*, 2018.
- [23] Decebal Constantin Mocanu, Elena Mocanu, Phuong H. Nguyen, Madeleine Gibescu, and Antonio Liotta. A topological insight into

- restricted Boltzmann machines. *Machine Learning*, 104(2-3):243–270, September 2016.
- [24] Grégoire Montavon, Alexander Binder, Sebastian Lapuschkin, Wojciech Samek, and Klaus-Robert Müller. *Layer-Wise Relevance Propagation: An Overview*, pages 193–209. Springer International Publishing, Cham, 2019.
- [25] Seyed-Mohsen Moosavi-Dezfooli, Alhussein Fawzi, and Pascal Frossard. Deepfool: A simple and accurate method to fool deep neural networks. In *2016 IEEE Conference on Computer Vision and Pattern Recognition (CVPR)*, pages 2574–2582, 2016.
- [26] Gregory Naitzat, Andrey Zhitnikov, and Lek-Heng Lim. Topology of deep neural networks. *Journal of Machine Learning Research*, 21(1), June 2022.
- [27] Maria-Irina Nicolae, Mathieu Sinn, Minh Ngoc Tran, Beat Buesser, Ambrish Rawat, Martin Wistuba, Valentina Zantedeschi, Nathalie Baracaldo, Bryant Chen, Heiko Ludwig, Ian Molloy, and Ben Edwards. Adversarial robustness toolbox v1.2.0. *CoRR*, 1807.01069, 2018.
- [28] Nicolas Papernot, Patrick D. McDaniel, Ian J. Goodfellow, Somesh Jha, Z. Berkay Celik, and Ananthram Swami. Practical black-box attacks against machine learning. In *Proceedings of the 2017 ACM on Asia Conference on Computer and Communications Security, AsiaCCS 2017, Abu Dhabi, United Arab Emirates, April 2-6, 2017*, pages 506–519. ACM, 2017.
- [29] Kevin Roth, Yannic Kilcher, and Thomas Hofmann. The odds are odd: A statistical test for detecting adversarial examples. In *Proceedings of the 36th International Conference on Machine Learning*, volume 97 of *Proceedings of Machine Learning Research*, pages 5498–5507. PMLR, 2019.
- [30] Eric Wong, Frank R. Schmidt, and J. Zico Kolter. Wasserstein adversarial examples via projected sinkhorn iterations. In *Proceedings of the 36th International Conference on Machine Learning*, volume 97 of *Proceedings of Machine Learning Research*, pages 6808–6817. PMLR, 2019.

- [31] Han Xu, Yao Ma, Hao-Chen Liu, Debayan Deb, Hui Liu, Ji-Liang Tang, and Anil K. Jain. Adversarial Attacks and Defenses in Images, Graphs and Text: A Review. *International Journal of Automation and Computing*, 17(2):151–178, April 2020.
- [32] Matteo Zambra, Amos Maritan, and Alberto Testolin. Emergence of network motifs in deep neural networks. *Entropy*, 22(2), 2020.